ChemComm

COMMUNICATION

View Article Online
View Journal | View Issue

Cite this: *Chem. Commun.*, 2026, **62**, 3560

Received 30th October 2025,
Accepted 12th December 2025

DOI: 10.1039/d5cc06192j

rsc.li/chemcomm

Effect of protonating single-moiety sulfonic acid-based dopants on the mechanical properties of electroconductive polyaniline/poly(2-acrylamido-2-methyl-1-propanesulfonic acid) complexes

Arya Ajeev,[a] Colton Duprey[b] and Evan K. Wujcik *[ab]

This comparative study investigates the role of side-group chemistry in mono-sulfonic acid dopants—CSA, DBSA, and TFMSA—within PANI/PAAMPSA complexes. The structural variations among the dopants significantly influenced the polymer-dopant interactions, which in turn altered key material properties. These findings provide molecular-level insights for developing highly stretchable, conductive, and autonomously self-healing materials for flexible and wearable applications.

The development of conductive polymer systems that integrate high electrical conductivity with robust mechanical stretchability remains a pivotal challenge for the advancement of next-generation flexible electronics.[1,2] Conducting polymers such as polyaniline (PANI) are a leading candidate for such applications, due to their excellent conductivity and environmental stability.[3] However, the inherent brittleness limits its use in scenarios that require mechanical deformation.[4] To overcome this limitation, PANI can be combined with intrinsically flexible polymer matrices, which impart the necessary stretchability to the system.[5]

The use of polymer acids, such as poly-2-acrylamido-2-methyl-1-propanesulfonic acid (PAAMPSA), as template and dopant, has proven effective in improving the mechanical integrity of PANI.[6,7] However, to further push the electrical and mechanical performance, secondary doping of this binary system is essential.[8] Although small molecule dopants with sulfonic acid groups have been explored, the specific influence of mono-sulfonic acids and their side group chemistry on interactions with the PANI/PAAMPSA complex remains unexplored.[9,10]

To create better conductive polymer systems, it is imperative to understand how the choice of side groups affects key properties like electrical behavior, molecular spacing, mechanical performance, water retention, *etc.* These factors collectively influence doping efficiency and interfacial interactions, which allow for the intentional design of polymers with improved performance. In this communication, we report the findings of the targeted investigation of the role of side-group chemistry using three structurally distinct mono-sulfonic acids: (1*S*)-(+)-10-camphorsulfonic acid (CSA), 4-dodecylbenzene sulfonic acid (DBSA), and trifluoromethane sulfonic acid (TFMSA).

Fig. 1a illustrates the *in situ* oxidative polymerization process used to synthesize PANI/PAAMPSA films doped with mono-sulfonic acids (MSAs). The synthesis consists of two key steps: polymerization and film casting. During the *in situ* polymerization step, ammonium persulfate (APS) serves as the initiator and helps to protonate aniline monomers and convert PANI from its insulating emeraldine base form to its conductive emeraldine-salt form, as evidenced by the green color of the resulting solution.[6] This process enables templated polymerization, where aniline monomers align with the negatively

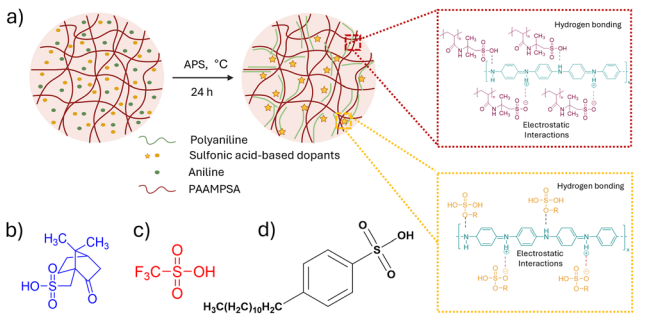

Fig. 1 (a) Schematic showing the synthesis process for the PANI/PAAMPSA/sulfonic acid polymer composite and the corresponding interactions between polyaniline chains with PAAMPSA and mono-sulfonic acids (b) structure of CSA (c) structure of TFMSA (d) structure of DBSA.

[a] *Materials Engineering and Nanosensor [MEAN] Laboratory, Department of Chemical and Biomedical Engineering, The University of Maine, Orono, Maine, USA. E-mail: Evan.Wujcik@maine.edu; Fax: +1 207-581-2323; Tel: +1 207-581-2742*

[b] *Advanced Structures and Composites Center [ASCC], The University of Maine, Orono, Maine, USA. E-mail: Colton.Duprey@maine.edu; Fax: +1 207-581-2323; Tel: +1 207-581-2742*

charged PAAMPSA backbone, facilitating zip-like polymerization, resulting in a head-to-tail chain growth within the doped complex. In this system, doping proceeds *via* a p-type protonic mechanism, where the imine nitrogen atoms of PANI are protonated by sulfonic acid groups (–SO_3H) of PAAMPSA and MSAs, forming positively charged iminium sites (–N^+H–) that electrostatically interact with anionic sulfonate groups (–SO_3^-). These ionic and hydrogen bonding interactions stabilize the doped polymer network, facilitate charge delocalization along the PANI backbone, and significantly enhance the electrical conductivity.[11] The introduction of structurally different MSAs further influences the morphology, chain organization, and packing, which leads to overall changes in the electrical and mechanical behavior of the resulting films.

The three MSAs possess distinct structural features that help to elucidate the structure–property relationships within the PANI/PAAMPSA systems. CSA (Fig. 1b) contains a rigid, bulky bicyclic terpene side group.[12] TFMSA (Fig. 1c) contains a highly electron-withdrawing CF_3 group,[13] whereas DBSA (Fig. 1d), an effective surfactant, features a long hydrophobic alkyl chain attached to a benzene ring.[14] Additionally, the sulfonic groups impart some polar characteristics, enabling it to interact with water. Fig. 2a shows the FTIR spectroscopy for PANI/PAAMPSA/MSAs. The bands at 1548 cm^{-1} and 1497 cm^{-1} correspond to the stretching vibrations of quinoid and benzenoid rings of PANI, respectively.[15] A characteristic polaron (electronic-like) band, associated with N═Q═N that confirms the doping appears at 1152 cm^{-1}.[16] The sulfonic acid bands are observed at 1174 cm^{-1}. The band at 3302 cm^{-1} is indicative of the –OH stretching. Compared to PANI/PAAMPSA/CSA and PANI/PAAMPSA/DBSA, the PANI/PAAMPSA/TFMSA peak is flattened, which can be attributed to the presence of stronger and more extensive hydrogen bonding present in the polymer matrix.[17]

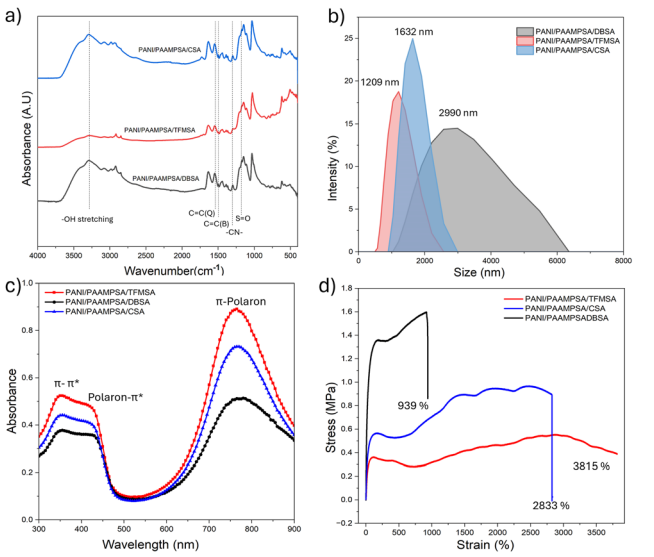

Fig. 2 (a) ATR-FTIR spectra of PANI/PAAMPSA doped with CSA, DBSA, and TFMSA (b) DLS particle size distributions of the three doped system (c) UV-Vis absorption spectra showing π–π*, polaron-π* and π-polaron transitions (d) stress–strain curves of the doped films.

The particle size analysis (Fig. 2b) revealed distinct distributions for each system: PANI/PAAMPSA/TFMSA showed the narrowest distribution (average size: 1209 nm), PANI/PAAMPSA/CSA was slightly broader (1632 nm), and PANI/PAAMPSA/DBSA showed a very broad distribution with a long tail extending to larger sizes. Consistently, the polydispersity index (PDI) follows PANI/PAAMPSA/CSA < PANI/PAAMPSA/TFMS < PANI/PAAMPSA/DBSA, with values of 0.084, 0.13, and 0.29, respectively, indicating the highest dispersion uniformity for CSA and the highest polydispersity for DBSA. The low PDI with CSA results from its rigid backbone, which enforces a more uniform, template-directed chain growth. The UV-Vis absorption spectra in Fig. 2c reveal the evolution of polaron band, the characteristic of the emeraldine-salt state. The absorption peak at ~350 nm corresponds to the π–π* transition of the benzenoid rings. A peak at ~420 nm represents the polaron-π* transition, while the peak at ~765 nm is attributed to the π-polaron transition, confirming the doped state of the quinoid rings.[18] The extent of the doping level can be estimated from the absorbance ratio of the π-polaron to the π–π* transition.[19] PANI/PAAMPSA/TFMSA showed the highest ratio (1.71), followed by PANI/PAAMPSA/CSA (1.65) and PANI/PAAMPSA/DBSA (1.37). The electrical conductivities of the films, as determined by a four-point probe measurement, were as follows: PANI/PAAMPSA/DBSA exhibited the highest value at 7.1×10^{-4} S cm^{-1}, followed by PANI/PAAMPSA/TFMSA (1.0×10^{-4} S cm^{-1}) and PANI/PAAMPSA/CSA (2.4×10^{-4} S cm^{-1}). The higher doping level of PANI/PAAMPSA/TFMSA does not necessarily yield the highest conductivity. This ratio indicates a higher carrier concentration (n), while electrical conductivity depends on both charge carrier concentration and mobility (μ).[20–22] Because of its amphiphilic nature, DBSA promotes microphase separation within the PANI/PAAMPSA complex. This results in a plasticized network with smoother, more continuous conductive pathways, thus enhancing carrier mobility.[23]

The elongation at break of the MSAs doped with PANI/PAAMPSA is shown in Fig. 2d. The PANI/PAAMPSA/TFMSA film exhibited the highest stretchability of 3477%. Remarkably, this film did not break, it exceeded the limit of the tensile testing machine. It showed a toughness of 16.13 MPa and a maximum stress of 0.5 MPa. PANI/PAAMPSA/CSA, despite its highly rigid and chiral structure, showed a stretchability of 2289%. The maximum stress achieved by this film is 0.96 MPa and the toughness is 22.03 MPa. The multiple strain-hardening of this film can be due to the sequential breaking and reformation of the ionic/hydrogen bond clusters, combined with progressive chain alignment.[24] The PANI/PAAMPSA/DBSA showed the lowest stretchability of 939%. However, it exhibited the highest elastic modulus (1.5 MPa) and a toughness of 13.10 MPa. Although DBSA is known for its surfactant like properties or plasticizing effect, the microphase separated morphology of DBSA creates stiff domains that can act as stress concentrators.[25] Instead of uniformly dissipating the energy through the network, the stress build up leads to earlier crack initiation and failure.[26] The small and non-bulky nature of the TFMSA dopant enables chain

slippage, helping to increase stretchability. In addition, the particle size distribution confirms a narrow distribution, so the stress will be evenly distributed throughout the material without localized stress concentration.[27] Thus, the strength of the PANI/PAAMPSA/TFMSA lies in its homogeneity, whereas the weakness of the PANI/PAAMPSA/DBSA film is its heterogeneity.

Thermal analysis of the PANI/PAAMPSA/MSAs is shown in Fig. 3a, revealing a three-stage degradation process. The initial stage (30–150 °C) is attributed to the loss of moisture, oligomers, free acids, and the residual initiator (APS). The second stage (150–320 °C) involves the loss of dopants, distortion of the main chain, and decomposition of the PAAMPSA side-chains. Finally, the third stage (320–780 °C) corresponds to the carbonization of the material. The determination of retained water in the film is essential, as this has significant direct influences on electromechanical properties. It is determined from the weight differential of ambient and dried sample at 150 °C, assuming that the majority of weight loss in this region arises from water evaporation.[3] PANI/PAAMPSA/DBSA retains the most water (13.84%, Fig. 3b), a result of its microphase-separated morphology, which enhances the material's capacity for water absorption.[28] A comparable water content of 11.22% and 11.62% was observed for PANI/PAAMPSA/CSA (Fig. 3c) and PANI/PAAMPSA/TFMSA (Fig. 3d), respectively. The lower water content of PANI/PAAMPSA/CSA is hypothesized to be due to the bulky rigid structure, reducing the free volume for the water molecules to occupy in the matrix. The self-healing efficiencies for the PANI/PAAMPSA/MSAs were evaluated on the basis of both electrical conductivity ($S.H\%_c$) and stretchability ($S.H\%_S$). This reveals the distinct self-healing capabilities of dopants in terms of physical integrity and electrical function. The equation followed for the self-healing efficiency calculation is given in the SI. All three dopants enabled autonomous self-healing in three hours. The separated halves were rejoined under ambient conditions, without requiring external triggers such as heat, pressure, or healing agents. The seamless rejoining of interfaces is critical for effective restoration of the material properties. The $S.H\%_c$ is given in the Fig. 4a. The $S.H\%_c$ of the films varied significantly with different mono-sulfonic acids. The PANI/PAAMPSA film with TFMSA dopant demonstrated the best overall performance, achieving perfect conductivity recovery (100%) and excellent stretchability recovery (91.14%) in three hours. The CSA-doped film also achieved 100% conductivity healing but a lower $S.H\%_S$ of 80.8%. In contrast, the DBSA-doped film showed markedly lower healing efficiencies, at 74.07% for conductivity and 21.82% for stretchability. The higher mechanical and conductivity recovery of PANI/PAAMPSA/TFMSA can be due to the compact CF_3 groups that enables tighter and uniform packing, and also the strong acid TFMSA allows for strong interactions with PANI/PAAMPSA that can reversibly dissociate and reform during mechanical deformation. This mechanism is supported by FTIR studies, which confirm the presence of strong hydrogen bonding, a key driver of the material's self-healing capability.[29] The lowest mechanical self-healing efficiency, demonstrated by PANI/PAAMPSA/DBSA, is likely due to its long hydrophobic tail not participating in the ionic bonding network, leading to a low density of effective healing sites, and causing structural heterogeneity that disrupts the effective reformation. Furthermore, phase separation likely weakens the film's overall mechanical integrity, further compromising its self-healing capability. PANI/PAAMPSA/CSA film exhibited moderate mechanical healing but full recovery of electrical conductivity. This suggests that conductive pathways can be easily re-established upon healing simply through physical contact of the polymer chains. However, lower stretchability healing is attributed to restricted chain mobility caused by the bulky and rigid CSA structure.

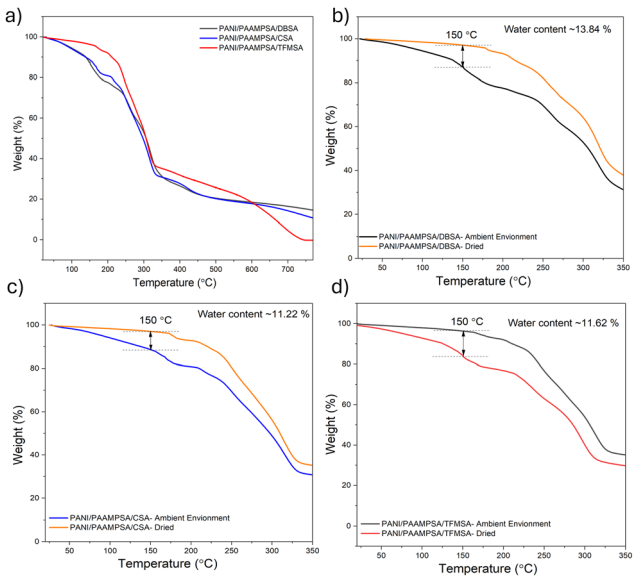

Fig. 3 (a) TGA analysis of PANI/PAAMPSA doped with MSA's from 30–780 °C under N_2. TGA thermogram of the ambient and dried (b) PANI/PAAMPSA/DBSA (c) d PANI/PAAMPSA/CSA (d) PANI/PAAMPSA/TFMSA.

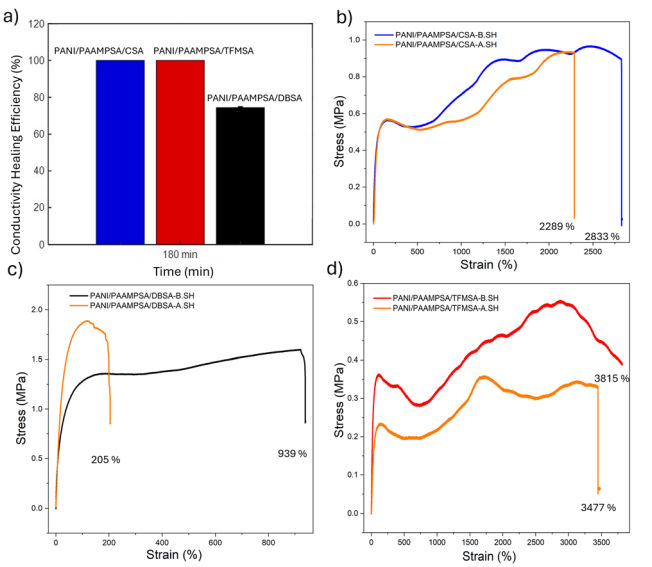

Fig. 4 (a) Conductivity self-healing efficiency of PANI/PAAMPSA/MSAs. Mechanical self-healing efficiency of (b) PANI/PAAMPSA/CSA (c) PANI/PAAMPSA/DBSA (d) PANI/PAAMPSA/TFMSA. The data plotted represents the mean and standard deviation (n = 3, n means number of independent experiments).

In conclusion, we have successfully developed highly stretchable, conductive, and autonomously self-healable films by doping PANI/PAAMPSA with mono-sulfonic acids- DBSA, CSA, and TFMSA. The side group chemistry of these acids played a crucial role in structural organization and resulting electro-mechanical behavior of the films. Among them, TFMSA, with its compact and strongly acidic nature, resulted in higher mechanical stretchability and self-healing capabilities within three hours. CSA, despite its bulky rigid structure, achieved complete electrical recovery but exhibited moderate mechanical healing, whereas the long hydrophobic chain of DBSA promoted phase separation, leading to diminished electrical and mechanical performance. Building on these insights, future studies will explore multi-sulfonic acid dopants to further enhance tunability in the PANI/PAAMPSA system with tunable properties and specific applications in durable wearable sensors and self-healing energy storage devices.

Conceptualization, funding acquisition, and project administration was carried out by E. K. W.; resources were provided by C. D.; investigation, visualization, and original draft writing was done by A. A.; methodology was conducted by C. D. and A. A.; reviewing & editing of the manuscript was carried out by A. A., C. D., and E. K. W.

E. Wujcik and A. Ajeev would like to acknowledge support from a National Science Foundation (NSF) CAREER Award from the Electronic/Photonic Materials program (NSF/MPS/DMR/EPM; award: 2305282).

Conflicts of interest

There are no conflicts to declare.

Data availability

The data supporting this article have been included as part of the supplementary information (SI). Supplementary information is available. See DOI: https://doi.org/10.1039/d5cc06192j.

Data will be made available upon request.

References

1 D. Davis, S. K. Narayanan, A. Ajeev, J. Nair, J. Jeeji, A. Vijayan, M. Viyyur Kuttyadi, A. Nelliparambil Sathian and A. K. Arulraj, *ACS Appl. Mater. Interfaces*, 2023, **15**, 25734–25743.
2 A. Ajeev, B. H. Javaregowda, A. Ali, M. Modak, S. Patil, S. Khatua, M. Ramadoss, P. A. Kothavade and A. K. Arulraj, *Adv. Mater. Technol.*, 2020, **5**, 2000690.
3 C. Duprey, A. Ajeev, D. Hong, K. Webb, S. Veres, G. Chen, E. Linn, G. Lusvardi, Z. Liu and R. Wang, *et al.*, *Adv. Compos. Hybrid Mater.*, 2025, **8**, 1–19.
4 M. Beygisangchin, A. H. Baghdadi, S. K. Kamarudin, S. A. Rashid, J. Jakmunee and N. Shaari, *Eur. Polym. J.*, 2024, **210**, 112948.
5 J. Bhadra, A. Alkareem and N. Al-Thani, *J. Polym. Res.*, 2020, **27**, 122.
6 Y. Lu, Z. Liu, H. Yan, Q. Peng, R. Wang, M. E. Barkey, J.-W. Jeon and E. K. Wujcik, *ACS Appl. Mater. Interfaces*, 2019, **11**, 20453–20464.
7 A. Ajeev, C. Duprey and E. K. Wujcik, *ACS Appl. Polym. Mater.*, 2025, **7**(21), 14562–14572.
8 A. H. Majeed, L. A. Mohammed, O. G. Hammoodi, S. Sehgal, M. A. Alheety, K. K. Saxena, S. A. Dadoosh, I. K. Mohammed, M. M. Jasim and N. U. Salmaan, *Int. J. Polym. Sci.*, 2022, **2022**, 9047554.
9 J. Huang and M. Wan, *J. Polym. Sci., Part A:Polym. Chem.*, 1999, **37**, 1277–1284.
10 J. Yue, Z. H. Wang, K. R. Cromack, A. J. Epstein and A. G. MacDiarmid, *J. Am. Chem. Soc.*, 1991, **113**, 2665–2671.
11 E. Matveeva, *Synth. Met.*, 1996, **79**, 127–139.
12 W. Oppolzer, *Tetrahedron*, 1987, **43**, 1969–2004.
13 R. Howells and J. Mc Cown, *Chem. Rev.*, 1977, **77**, 69–92.
14 H. Najari and A. Sanati, *J. Mol. Liq.*, 2024, **400**, 124548.
15 M. Trchová, I. Šeděnková, E. Tobolková and J. Stejskal, *Polym. Degrad. Stab.*, 2004, **86**, 179–185.
16 C. Zhou, Y. Ren, J. Han, Q. Xu and R. Guo, *ACS Nano*, 2019, **13**, 3534–3544.
17 Y. He, B. Zhu and Y. Inoue, *Prog. Polym. Sci.*, 2004, **29**, 1021–1051.
18 D. Y. Imali, E. C. J. Perera, M. Kaumal and D. P. Dissanayake, *RSC Adv.*, 2023, **13**, 6396–6411.
19 T. Abdiryim, R. Jamal and I. Nurulla, *J. Appl. Polym. Sci.*, 2007, **105**, 576–584.
20 J. Lim, M. Kober-Czerny, Y.-H. Lin, J. M. Ball, N. Sakai, E. A. Duijnstee, M. J. Hong, J. G. Labram, B. Wenger and H. J. Snaith, *Nat. Commun.*, 2022, **13**, 4201.
21 S. Wang, C. Chang, S. Bai, B. Qin, Y. Zhu, S. Zhan, J. Zheng, S. Tang and L.-D. Zhao, *Chem. Mater.*, 2023, **35**, 755–763.
22 M. Koopmans, M. A. Leiviska, J. Liu, J. Dong, L. Qiu, J. C. Hummelen, G. Portale, M. C. Heiber and L. J. A. Koster, *ACS Appl. Mater. Interfaces*, 2020, **12**, 56222–56230.
23 B. Yang and Z. Cunman, *Chem. Eng. J.*, 2023, **457**, 141094.
24 W. Hong, J. Lin, X. Tian and L. Wang, *Polymer*, 2021, **235**, 124301.
25 S. Minu, R. Ramani, R. I. Shekar, T. M. Kotresh and N. V. Padaki, *Soft Matter*, 2022, **18**, 7380–7393.
26 T. Kang, J. Dai, Y. Huang, H. Kim, S. Keten and J. Kim, *Chem. Rev.*, 2025, **125**(22), 11032–11057.
27 S.-Y. Fu, X.-Q. Feng, B. Lauke and Y.-W. Mai, *Composites, Part B*, 2008, **39**, 933–961.
28 S. H. van Leuken, J. J. van Gorp, R. A. van Benthem, M. Vis and R. Tuinier, *Fluid Phase Equilib.*, 2025, **588**, 114233.
29 C. Lu, Z. Ling, C. Wang, J. Wang, Q. Yong and F. Chu, *Composites, Part B*, 2022, **228**, 109428.